Inorganic Chemistry
Article
pubs.acs.org/IC

Synthesis, Ab Initio X-ray Powder Diffraction Crystal Structure, and Magnetic Properties of $Mn_3(OH)_2(C_6H_2O_4S)_2$ Metal−Organic Framework

Romain Sibille,*[†] Thomas Mazet,[†] Erik Elkaïm,[‡] Bernard Malaman,[†] and Michel François[†]

[†]Université de Lorraine, Institut Jean Lamour−UMR 7198, BP 70239, 54506 Vandoeuvre-lès-Nancy Cedex, France
[‡]Synchrotron SOLEIL, L'Orme des Merisiers, Saint-Aubin, BP 48, 91192 Gif-sur-Yvette Cedex, France

Supporting Information

ABSTRACT: A new hydroxythiophenedicarboxylate metal−organic framework based on Mn^{II} cations has been obtained by an aqueous two-step procedure including hydrothermal treatment. The structure of $Mn_3(OH)_2(C_6H_2O_4S)_2$ has been determined ab initio from synchrotron X-ray powder diffraction data and consists of infinite inorganic ribbons which are interlinked by 2,5-thiophenedicarboxylate (tdc) molecules (monoclinic, space group $P2_1/c$, $a = 3.4473(1)$ Å, $b = 19.1287(1)$ Å, $c = 11.0069(1)$ Å, $\beta = 97.48(1)°$, $V = 719.65(1)$ Å^3, and $Z = 2$). Each ribbon is built of three vertex-sharing chains of edge-sharing MnO_6 octahedrons. These ribbons are bridged together by the carboxylate functions of the tdc molecule to form a pseudo-2D inorganic subnetwork, while this molecule develops in the third dimension to pillar these pseudo-2D layers. An unprecedented hexadentate symmetric bridging mode is adopted by tdc which bridges two chains of a ribbon on one side and two ribbons of a pseudo-2D inorganic subnetwork on the other side. Magnetic measurements suggest that the titled compound is antiferromagnetic below $T_N = 17.7$ K. Heat capacity measurements confirm the existence of a magnetic phase transition toward a 3D long-range ordered state. These $C_P(T)$ data have also been used for the calculation of the thermal variations of both the adiabatic temperature change ΔT_{ad} and magnetic entropy change ΔS_m of the material, namely its magnetocaloric effect.

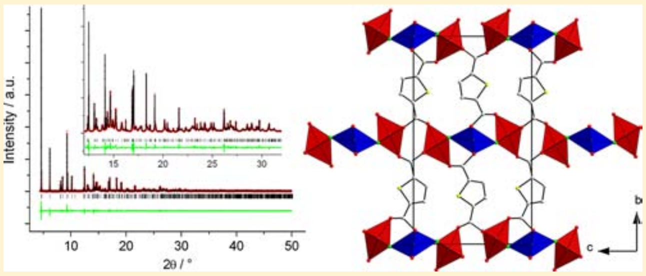

■ INTRODUCTION

The field of metal−organic framework (MOF) materials continues to expand at a remarkable pace,[1] in part because of the limitless number of possibilities offered by the combination of organic and inorganic building blocks, but also because of their ability to produce interesting properties for both industrial applications and fundamental science. This growing class of materials has been studied for numerous applications including gas storage and separation,[2] catalysis,[3] ion sensing[4] or luminescence.[5] By their unique structural and composition diversities, MOF materials are also a huge source of experimental systems for exploring magnetism.[6] In magnetic MOFs, the organic moiety can either act as a simple spacer between spin clusters, chains, or layers, or as an active component of the whole material. In the former case, magnetically inert molecules such as alkane chains can be used for tuning distances between spin systems.[7,8] In the latter case, it can lead up to the juxtaposition of different properties in the same material or to new properties by a synergic interplay between the organic and the inorganic subnetworks. For this, more complex molecules, aromatic ones often, are of great interest.

Among the various types of ligands used to design MOFs, carboxylates are especially well-placed[9] because of their robustness and the relatively easy access to functional molecules bearing carboxylate groups. In this group of ligands, thiophenecarboxylates are particularly interesting in materials science because of their aromaticity. They have been used because of their ability to transfer efficiently the energy of their π, π* excited state to 4f cations to increase their luminescence quantum yield in polymers,[10] lanthanide complexes,[11,12] or MOFs.[13−16] In addition, the quest for multifunctionality has motivated recent works on molecular magnetic compounds mixing magnetic cations and thiophenecarboxylates ligands. The examples concern the grafting of thiophenemonocarboxylates[17] and thiophenedicarboxylates[18] into layered transition-metal hydroxides obtained by anionic exchange reaction, as well as the direct synthesis of MOFs with thiophenedicarboxylates and 3d[18−20] or 4f[13,15] magnetic cations. In these examples the functionalities of the obtained materials were luminescence and magnetism. There is also an example for which oligothiophenedicarboxylates were used for the bridging of Mn_6 single-molecule magnets (SMMs) to combine magnetic and redox properties.[21]

Received: July 2, 2012
Published: December 28, 2012

In the case of the direct synthesis of MOFs, the shorter thiophenedicarboxylate, namely, 2,5-thiophenedicarboxylate (tdc), has taken a major place because of its good solubility in various solvents. In these tdc-based materials, this linker can either acts as the only ligand[13,14,19,20,22,23] in combination with small O-donor or N-donor molecules (hydroxide,[19] water,[19,20,14,13,23] methanol,[13] ethanol[13] and dimethylformamide[13,22]), or as a coligand[15,16,24,25] in combination with other large ligands (pyridine,[23] bipyridine,[23,25,26] phenantroline,[23] 1,3-bis(4-pyridyl)propane,[24,27] oxalate,[15] 1-methyl-3-ethylimidazolium[16] and propane-1,3-diamine[28]). The rich structural diversity found in MOFs containing tdc has been attributed to its "V-shaped" configuration yielding various coordination modes.[13,15] Among MOFs including tdc, one can distinguish $Ni_3(OH)_2(tdc)_2(H_2O)_4$ as the only one containing hydroxide groups.[19] Hydroxy-dicarboxylates materials are generally not obtained as single-crystals and, consequently, this is also the only example of tdc-based MOF for which the structure was solved ab initio from synchrotron X-ray powder diffraction (XRPD) data. One can remark that the compounds containing only the three following constituents "3d transition metal—hydroxide—dicarboxylate" seem to be more difficult to obtain with tdc than with other dicarboxylates being "linear-shaped" such as 1,4-benzenedicarboxylate (bdc).[29] Here we report a first example in this system, namely, $Mn_3(OH)_2(C_6H_2O_4S)_2$. We present its synthesis, crystal structure solved from synchrotron XRPD data, topological representation, and magnetic properties. We also report about the unprecedented coordination mode of tdc in this material.

EXPERIMENTAL SECTION

Synthesis. All chemicals were commercially available from Aldrich and used as received. $Mn_3(OH)_2(C_6H_2O_4S)_2$ was synthesized according to the following procedure: thiophene-2,5-dicarboxylic acid (1.5 mmol, 0.26 g) was dissolved into 10 mL of distilled water. The pH of the starting solution was finely adjusted by NaOH droplets to 9.0. The resulting solution was placed into a homemade 50 mL plastic reactor under constant argon current to avoid the formation of manganese oxide impurities. This hermetic reactor was equipped with two injectors, a pH electrode, and magnetic stirring. The system was deoxygenated for 10 min before the combined addition of the $MnCl_2{\cdot}4H_2O$ (1 mmol, 0.20 g in 8 mL of water) and NaOH (≈ 2 mmol, 10 mL 0.2 M) solutions by the two injectors. The addition was driven by two peristaltic pumps (*Ismatec*) and the electrode was linked to a pH-meter (*Knick*). The two peristaltic pumps and the pH-meter were driven by a computer via the Labworldsoft program. The addition of the metallic salt solution was done at a constant rate while the addition rate of the basic solution was varied to keep a constant pH during the whole course of the addition (1 h 30). After this first step, the mixture was stirred for five more minutes and then sucked up by a syringe which was then transferred into a glovebox under argon atmosphere. The mixture was finally transferred into a Teflon-walled stainless steel autoclave under the argon atmosphere. Following this first step, the titled compound was obtained by a hydrothermal treatment at 150 °C. After three days, the autoclave was naturally cooled in air and opened under ambient atmosphere. The powdered reaction product was collected by centrifugation, washed twice with a mixture of distilled water and ethanol (1/1), and then dried at room temperature. Yield (based on manganese): 72%.

Characterization Methods. Thermogravimetric measurement was performed using a Setaram TGDTA-92 thermobalance. Samples were placed in alumina containers, and data were recorded in air between 25 and 550 °C, with a heating rate of 1 °C/min. The data were corrected for the empty container. FTIR spectrum was obtained with a Bruker Vertex 80v spectrometer in the region 500–4000 cm^{-1}. Samples were prepared as disks of dried KBr (100 mg) mixed with a small amount of the sample (3 mg). A dried KBr disk was used as baseline correction. Laboratory XRPD data were collected at room temperature using filtered Cu Kα radiation (λ = 1.5418 Å) and a reflection Bragg–Brentano θ-θ geometry (Philips X-Pert Pro diffractometer). Magnetic susceptibility measurements were carried out with a MPMS VSM-SQUID Quantum Design magnetometer between 2 and 300 K. The 2.7 mg polycrystalline specimen was placed into a commercial Quantum Design sample holder. The magnetic response was corrected with a diamagnetic blank data of the sample holder obtained separately, and the diamagnetic contribution of the sample itself was estimated from Pascal's constants. Heat capacity measurements were recorded with a PPMS-9T Quantum Design apparatus equipped with the heat capacity module as well as with a cryopump that allows working under secondary vacuum. Data were obtained in the temperature range [2.3–80 K] under various direct current (dc) fields. The addenda were first recorded for the heat capacity platform and for the grease (Apiezon N) which was used to fix a 2.6 mg polycrystalline sample on the heat capacity platform. In these conditions, the sample contribution to the total heat capacity signal was 0.68 (80 K) to 29.3 (2.3 K) times the addenda contribution.

Sample Homogeneity. All physical measurements were carried out with the sample used for the XRPD structure determination. No significant impurity was seen in these measurements. Furthermore, thermogravimetric analysis (TGA) and chemical analysis were used. The TGA trace (Supporting Information, Figure S2) shows decomposition in air above 350 °C. The weight loss occurs in a single step up to 425 °C and related to the degradation of the tdc molecules (57.0% observed ; 56.1% calculated for the reaction 1 $Mn_3(OH)_2(C_6H_2O_4S)_2$ gives 1.5 Mn_2O_3). The good thermal resistance of $Mn_3(OH)_2(C_6H_2O_4S)_2$ confirms the absence of water molecules in the compound formula and indicates that a strong bond interaction between organic and inorganic components has been achieved by the hydrothermal process. The purity of the Mn_2O_3 residue was checked by XRPD (PDF: 071-0636). Chemical analysis: $C_{12}H_6Mn_3O_{10}S_2$ (539.1 g·mol^{-1}) Anal. (Calcd): C, 25.98 (26.71); O, 29.18 (29.68); Mn, 31.04 (30.57); S, 12.67 (11.90).

Synchrotron XRPD. High-resolution XRPD data were collected at ambient temperature with synchrotron radiation at SOLEIL (Saint Aubin, France), on the CRISTAL beamline. A monochromatic beam was extracted from the U20 undulator beam by means of a Si111 double monochromator. Its wavelength (λ = 0.77752 Å) was refined from a LaB6 (NIST Standard Reference Material 660a) powder diagram recorded just before the experiment. The high angular resolution is obtained using a two circles diffractometer (SMP–Lyon) equipped with a 21 perfect crystals Si(111) multianalyzer. The sample enclosed in a capillary (Φ = 0.8 mm) is mounted on a spinner rotating at about 5–10 Hz to improve powder averaging. Patterns were recorded for 2 h in the angular range $4 < 2\theta < 50°$ with an interval of 0.002°. Transmission of the filled capillary was measured using an X-ray camera allowing us to fix a reliable μr value of 0.345 during the Rietveld refinement.

Structure Determination. Laboratory XRPD data were used in a first time. A set of 20 Bragg peaks were manually determined using the Winplotr application implemented in the Fullprof program.[30] This set of data was used for running the trial and error indexing procedure of the TREOR90 program.[31] A second indexing procedure was performed by the means of the successive dichotomy method with the DICVOL04 program[32] using the same set of peaks. A common solution was found in the monoclinic system with a = 3.4475 Å, b = 19.1368 Å, c = 11.0146 Å, and β = 97.455°. The possible space groups were examined using the Fullprof program running in the "profile matching" mode (Le Bail decomposition).[33] The careful analysis of the systematic extinctions led to retain the $P2_1/c$ space group. Through knowledge of the unit cell parameters and experimental weight loss, an initial model was found by direct-space methods using the FOX program.[34,35] The initial model was found with the following scatterers in the unit cell: one tdc molecule defined as a "rigid body" whose orientation and position are free and two MnO_6 octahedrons, one having free orientation and position and the other one having a free orientation but a central atom fixed on the 2a special position. The global optimization procedure was using the parallel tempering algorithm.

Then the high-resolution synchrotron XRPD data were first used in the "profile matching" mode of Fullprof to refine the cell and profile parameters. The LaB_6 standard was used to define the instrumental resolution function. The peak shape profiles were defined by using the Thomson−Cox−Hasting pseudo-Voigt function for the sample contribution. Nine crystallite size effects parameters (spherical harmonics) were refined to characterize the anisotropic broadening of the peaks. The Rietveld refinement includes 58 intensity dependent parameters. H atoms were geometrically placed and fixed before the final Rietveld refinement of the 75 parameters. No constraints were applied, and the background was defined using linear interpolation between a set of fixed points. The resulting crystallographic and refinement parameters are given in Table 1, and the final Rietveld plot is presented in Figure 1. Figure 2 shows that the use of an anisotropic peak broadening model has proved indispensable to fit the synchrotron data.

Table 1. Crystal Data and Rietveld Refinement Parameters

Crystal Data	
formula	$Mn_3(OH)_2(C_6H_2O_4S)_2$
molecular weight	539.12 g·mol^{-1}
Z	2
space group	$P2_1/c$
a	3.4473(1) Å
b	19.1287(1) Å
c	11.0069(1) Å
β	97.48(1)°
V	719.65(1) Å^3
ρ_{calc}	2.49 g cm^{-3}
Rietveld Refinement Parameters	
2θ range (wavelength)	4.4−50° (0.77752 Å)
absorption coefficient ($\mu \times r$)	0.345
$N_{obs.\ points}$	22799
$N_{reflexions}$	1137
$N_{intensity\text{-}dependent\ parameters}$ ($N_{profile\ parameters}$)	58 (17)
R_p (R_{wp})	0.0828 (0.1140)
R_{Bragg}	0.0430
R_F	0.0405

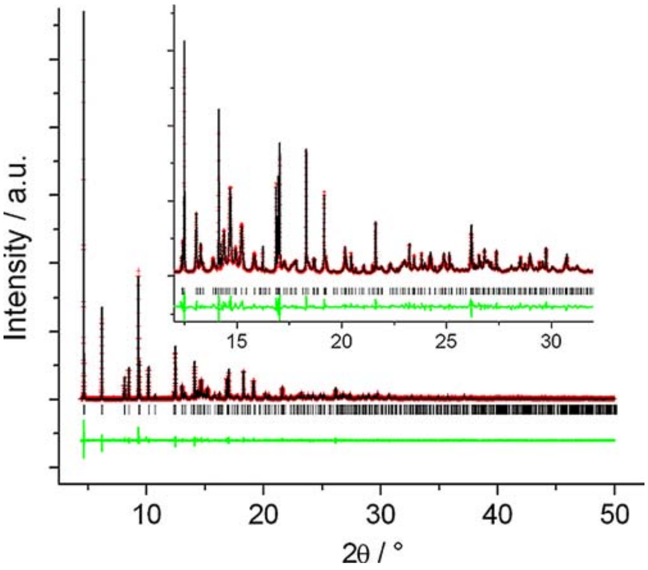

Figure 1. Observed (red), Rietveld calculated (black), and difference (green) synchrotron XRPD patterns (λ = 0.77752 Å). The vertical bars indicate the Bragg positions.

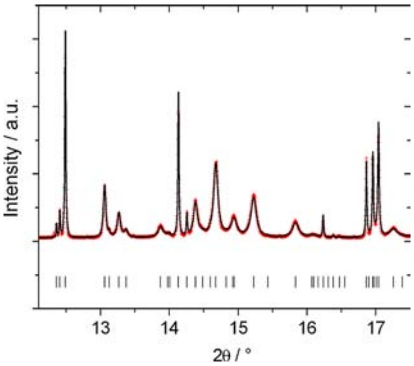

Figure 2. Part of the observed (red) and Rietveld calculated (black) synchrotron XRPD patterns (λ = 0.77752 Å) illustrating the anisotropic peak broadening attributed to particle size effects.

■ RESULTS AND DISCUSSION

Crystal Structure. The $Mn_3(OH)_2(C_6H_2O_4S)_2$ MOF crystallizes in the monoclinic $P2_1/c$ space group (see Table 1 and Figure 3) and the asymmetric unit consists of two Mn(II) ions, one hydroxide group, and one tdc molecule.

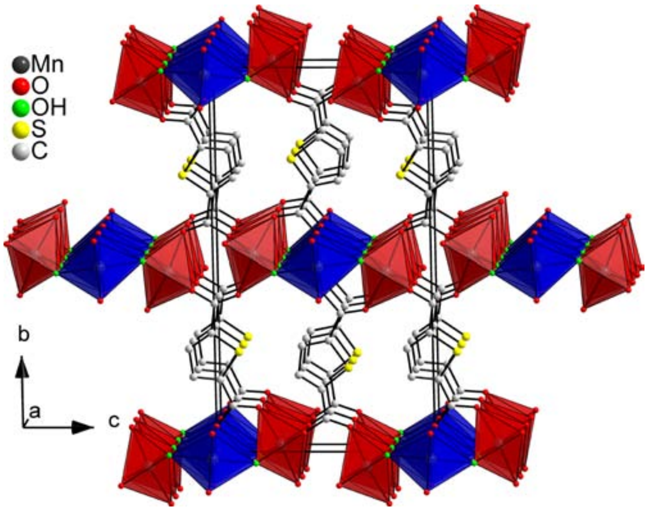

Figure 3. General view of the crystal structure of $Mn_3(OH)_2(C_6H_2O_4S)_2$ MOF. Hydrogen atoms have been omitted for clarity. Mn1 and Mn2 metallic sites are represented by the red and blue polyhedrons, respectively.

The inorganic subnetwork is made of manganese-based 1D ribbons running along the **a** axis (Figure 4). These ribbons are built of three infinite chains of MnO_6 octahedrons. The three chains that constitute a ribbon are of two types, the central one is made of edge-sharing oxygen octahedrons centering the Mn2 site while the two adjacent chains are built up from edge-sharing oxygen octahedrons centering the Mn1 site. The two crystallographically independent manganese sites Mn1 and Mn2 are in general position (Wickoff position 4*e*) and in special position (Wickoff position 2*a*), respectively. For Mn2 site, the equatorial plane of $Mn2O_6$ site octahedron is formed by four O atoms coming from four distinct tdc molecule. This equatorial plane is tilted by an angle of about 5° from the (a,b) plane. The two apical O atoms of the $Mn2O_6$ octahedron come from hydroxide groups. Each of these apical O atoms is almost oriented along **c**-axis from Mn2. These apical atoms of $Mn2O_6$ octahedron are shared with two octahedrons of an adjacent

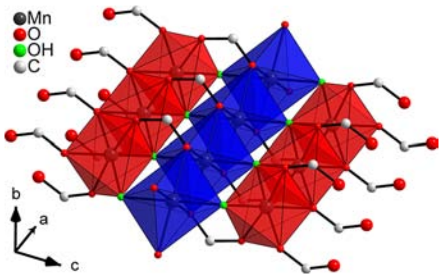

Figure 4. View of the 1D inorganic subnetwork in $Mn_3(OH)_2(C_6H_2O_4S)_2$ MOF. Hydrogen atoms have been omitted for clarity. Mn1 and Mn2 metallic sites are represented by the red and blue polyhedrons, respectively. Both the intra- and inter-ribbon carboxylato bridges are represented.

$Mn1O_6$ chain. Consequently, the hydroxide group acts as a μ_3-OH^- group assembling the chains forming the ribbons. The equatorial plane of $Mn1O_6$ octahedron is formed by two O_{OH} and two O_{COO} from two distinct tdc molecules. This equatorial plane is tilted by an angle of about 31° from the (a,c) plane. Both apical O atoms of the Mn1 site are in turn coming from the carboxylate functions of tdc molecules. The tilt angles defined for both metallic sites between the equatorial plane of the octahedron and a crystallographic plane are conserved for each ribbon within the same (a,c) layer, while they are reversed upon going from an (a,c) layer to the next one in the [010] direction, as a result of the screw axis. The interatomic distances of interest within the inorganic ribbons are given in Table 2.

Table 2. Summary of the Interatomic Distances in the 1D Inorganic Subnetwork of $Mn_3(OH)_2(C_6H_2O_4S)_2$ MOF

	$Mn2O_6$			$Mn1O_6$	
Mn2	O_{COO}	2.225 Å	Mn1	O_{COO}	2 × 2.222 Å
	O_{COO}	2.317 Å		O_{COO}	2 × 2.316 Å
	O_{COO}	2.148 Å		O_{OH}	2 × 2.156 Å
	O_{COO}	2.135 Å			
	O_{OH}	2.197 Å			
	O_{OH}	2.196 Å			
Mn2	Mn2	3.433 Å	Mn1	Mn2	3.633 Å
Mn1	Mn1	3.433 Å	Mn1	Mn2	3.785 Å

The 1D inorganic subnetwork described so far is interlinked by the means of a unique tdc molecule to form a 3D framework. On one side, this tdc molecule bridges the adjacent ribbons of the same (a,c) layer, while on the other side the carboxylate function bridges two adjacent chains of a ribbon. Strictly speaking the material should be described as an I^1O^2 framework according to the simple notation I^mO^n where m and n stand for the dimensionality of the inorganic and organic connectivity, respectively.[36] However, the infinite (a,c) layers formed by an array of carboxylato-bridged ribbons could also be defined as a pseudo-2D inorganic subnetwork reflecting the layered nature of this material.

The connection of the tdc molecule with the inorganic subnetwork can be summarized by the symmetric hexadentate $(\kappa^1\text{-}\kappa^1\text{-}\mu_2)\text{-}(\kappa^1\text{-}\kappa^1\text{-}\mu_2)\text{-}\mu_6$ bridging mode. The complete formula of the compound can thus be written as $Mn_3[\mu_3\text{-}OH]_2[(\kappa^1\text{-}\kappa^1\text{-}\mu_2)\text{-}(\kappa^1\text{-}\kappa^1\text{-}\mu_2)\text{-}\mu_6\text{-}C_6H_2O_4S]_2$. The bridging mode found here is unprecedented for the tdc linker. Supporting Information, Scheme S1 summarizes, to the best of our knowledge, all the coordination modes observed for tdc in MOFs and coordination polymers[13−16,19,20,22−28] or complexes,[37−43] as well as the new one found in $Mn_3(OH)_2(C_6H_2O_4S)_2$ MOF. The final geometry of tdc obtained here from synchrotron XRPD data (without any constraints) compares very well with that of the optimized molecule (see Supporting Information, Figure S6).

FTIR. The Fourier Transform InfraRed spectrum (Figure 5) shows the characteristic stretching vibrations of OH^-, COO^- and aromatic CH groups. A sharp band at 3588 cm^{-1} is assigned to the stretching vibration of OH groups not involved in hydrogen bonding. The band found at 3110 cm^{-1} is attributed to the stretching vibration of the C_{sp2}−H groups borne by the thiophene ring. The inset of Figure 5 shows a band at 1522 cm^{-1} which is assigned to the antisymmetric stretching vibration of the carboxylate function ($\nu_{as}(COO^-)$). This band was recorded at 1560 cm^{-1} in Na_2tdc.[19,20] The spectrum of $Mn_3(OH)_2(C_6H_2O_4S)_2$ also clearly displays an intense and broad feature centered around 1350 cm^{-1} which is attributable to the symmetric stretching mode of the carboxylate functions ($\nu_s(COO^-)$). Compared with Na_2tdc in which this band was unique and found at 1385 cm^{-1}, $\nu_s(COO^-)$ seems to be split in four distinct bands in $Mn_3(OH)_2(C_6H_2O_4S)_2$: 1331, 1342, 1358, and 1373 cm^{-1}. These various frequencies may be related to the bridging mode of the carboxylate functions of tdc in this compound since, although the coordination mode of tdc is symmetric, the two carboxylate functions bridge respectively two chains of a ribbon and two ribbons of a pseudo-2D inorganic subnetwork. The small splitting ($\Delta\nu_{as\text{-}s}$ = [149−191 cm^{-1}]) between the carboxylate-stretching frequencies is characteristic of bridging carboxylates, in accordance with the crystallographic structure of the compound.

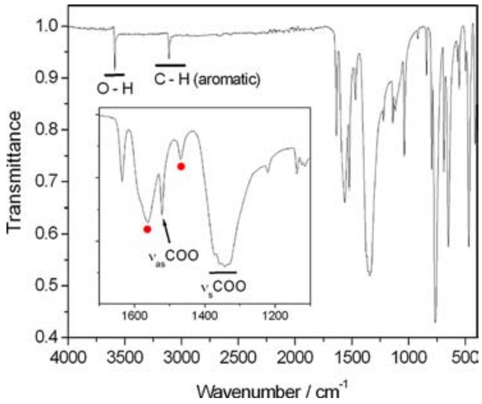

Figure 5. FTIR spectrum recorded in transmission. The red circles in the inset designate the bands attributed to in-plane ring vibrations of the tdc molecule.

Topological Description. The framework can be simplified by the application of a 4-nodal topological approach (Figure 6).[44] The metallic ions define two inorganic nodes, and the carbon atoms of the carboxylate functions define two organic nodes. Figure 6 (right) gives a view from the top of two adjacent ribbons. This view evidences the fact that the metallic ions form a triangular net within a ribbon. The 3D framework resulting from the adequate connection of organic nodes is shown in Figure 6 (left). One can easily see from Figure 6 that one of the two organic nodes has an intraribbon character, while the other one links two adjacent ribbons in the (a,c)

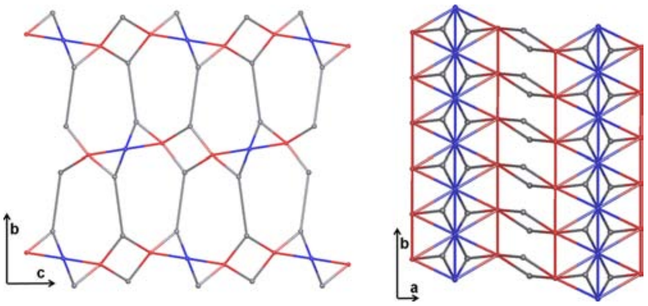

Figure 6. Topological representation of $Mn_3(OH)_2(C_6H_2O_4S)_2$ MOF. The red and blue nodes represent Mn1 and Mn2 ions, respectively. The gray nodes represent the two independent carboxylic functions of the molecule. The right part of the figure shows the connection of two ribbons.

plane. This topological framework is a (3,4,7,10)-connected net with stoichiometry $(3\text{-c})_2(4\text{-c})_2(7\text{-c})_2(10\text{-c})$. The point symbol for this net is $(3^{14}.4^{16}.5^{13}.6^{2})(3^{7}.7^{3})_2(3^{5}.4^{5}.5.6^{4}.7^{5}.8)_2(4.7^{2})_2$.

Magnetic Properties. The thermal dependence of the static magnetic susceptibility χ_{dc} has been recorded for an applied magnetic field $\mu_0 H_{dc}$ of 0.1 T (Figure 7a). It is characteristic of an antiferromagnetic behavior: upon decreasing temperature, χ_{dc} increases continuously, reaches a maximum at $T_N = 17.7$ K before it decreases again. The antiferromagnetic character of this transition is corroborated by the occurrence of a peak in the in-phase component of the dynamic magnetic susceptibility χ_{ac} without any corresponding signal in the out-of-phase component (Figure 7b). No frequency dependence of this ac signal is observed.

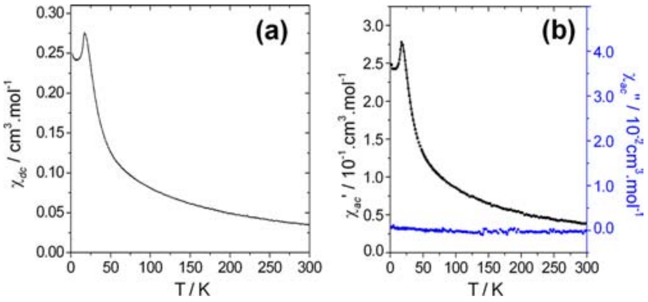

Figure 7. Thermal dependencies: (a) static magnetic susceptibility (χ_{dc}) recorded under an applied magnetic field $\mu_0 H_{dc} = 0.1$ T. (b) Real and imaginary parts of the dynamic magnetic susceptibility (χ_{ac}) recorded with an oscillating field $\mu_0 H_{ac}$ of 0.5 mT ($\nu_{ac} = 1000$ Hz).

The data in the temperature range of 60−300 K obeys the Curie−Weiss law $\chi = C/(T - \theta)$ with $C = 13.89$ cm^3 K mol^{-1} (or equivalently $C = 4.63$ cm^3 K Mn(II) mol^{-1}) and $\theta_p = -68.2$ K (Figure 8a). This large paramagnetic temperature is indicative of dominant antiferromagnetic interactions in the paramagnetic region. The deduced Curie constant per mole of Mn(II) agrees with the theoretical value of an $S = 5/2$ free ion ($C = 4.38$ cm^3 K Mn(II) mol^{-1}). The corresponding experimental effective magnetic moment for Mn(II) in $Mn_3(OH)_2(C_6H_2O_4S)_2$ is 6.08 μ_B (theoretical value: 5.92 μ_B). The thermal evolution of the $\chi_{dc}T$ product in the temperature range of 2−300 K is presented Figure 8b. The room temperature value equals 12.95 cm^3 K mol^{-1}, close to the expected value for three Mn(II) free ions (13.14 cm^3 K mol^{-1}). Figure 8b also shows the fit of the experimental data by the exponential function $\chi T = C \times \exp(E/kT)$ in the temperature domain 60−300 K. The best fit gives $C = 14.96$ cm^3 K mol^{-1}, the Curie constant, and $E/k = -44.65$ K, the overall exchange coupling energy within the magnetic layers (J_{intra}). Of course, this latter value can only have an average meaning over the numerous pathways able to carry magnetic exchanges within the (a,c) layers. A perfectly exponential variation of the χT product would be characteristic of a 2D Heisenberg system.[45] Here, we should note that the use of this model gives an imperfect fit over the measured paramagnetic domain. This is likely because, at high temperature, correlations may develop along the ribbons while the inter-ribbon interactions should remain negligible.

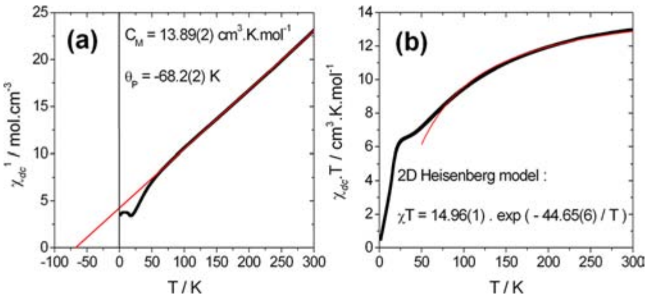

Figure 8. Analysis of the experimental static magnetic susceptibility (χ_{dc}). (a) Plot of $\chi_{dc}^{-1}(T)$ (black) and the Curie−Weiss fit (red). (b) Plot of $\chi_{dc}T(T)$ (black) and the best fit to the exponential function of the 2D Heisenberg model (red). In both cases the fit is limited to the 60−300 K temperature range.

Figure 9 shows isothermal magnetization cycles recorded at 5 and 25 K in the [−7 T, 7 T] range, both in magnetic field increase and decrease. It is seen that the field dependence of the magnetization departs from the linear behavior expected for a simple antiferromagnet. A change of slope is observed at $\mu_0 H_c \approx 2.9$ T, which manifests itself by a peak in the field derivative of the magnetization (inset of Figure 9). This metamagnetic-like transition can be due to a spin-flop process characteristic of such an antiferromagnetic system with a weak magnetic anisotropy. Above this threshold field, the magnetization does not saturate and remains well below the 15 μ_B mol^{-1} of three aligned Mn(II) spins. There is no significant magnetic hysteresis in the recorded data.

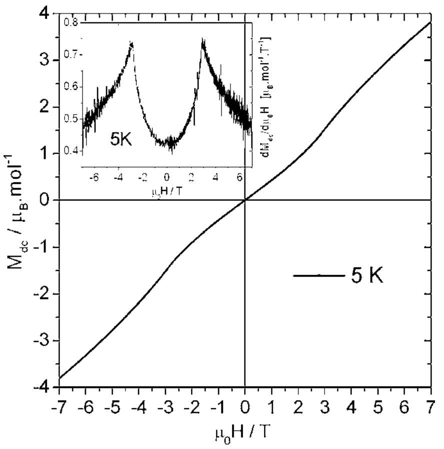

Figure 9. Isothermal magnetization curves. Magnetization cycle in the ordered state (5 K). The inset represents the derivative.

Magnetothermal Properties. Heat capacity measurements have been carried out in the [2.3−80 K] temperature range to confirm the existence of a long-range ordered (LRO) state below T_N. The $C_P(T)$ curve recorded under zero-field (Figure 10) shows a λ-type peak anomaly at 16.3 K which provides a clear evidence of the realization of a 3D LRO state through a second-order transition. Its reduced height is due to the relatively weak interlayer magnetic interactions.[46] The inflection point of $C_P(T)$ data in zero-field, which has been suggested to most adequately represent the magnetic ordering temperature,[47] is found at 16.7 K, in reasonable agreement with the Néel temperature of 17.7 K deduced from magnetic measurements. Upon field increase, the λ-peak smears out and shifts to lower temperature, as expected for a phase transition toward an antiferromagnetic state. The magnetocaloric effect (MCE) of $Mn_3(OH)_2(C_6H_2O_4S)_2$ was evaluated from these C_P data. The MCE, which scales with the temperature derivative of the magnetization, corresponds to the adiabatic temperature change (ΔT_{ad}) or the magnetic entropy change (ΔS_M) of a magnetic solid in a varying magnetic field.[48] The MCE can serve as a tool for investigating basic aspects of a magnetic material,[8,48] but may also be exploited using paramagnetic-like materials in low-temperature refrigeration applications (e.g., adiabatic demagnetization refrigerators[49]) when their magnetic susceptibility almost diverges and, consequently, their MCE is strong. The isothermal magnetic entropy change $-\Delta S_M$ (Figure 11a) and adiabatic temperature change ΔT_{ad} (Figure 11b) were calculated from the measured heat capacity in various magnetic fields as described in ref 50. The total entropy of a magnetic solid in a given field can be calculated from the heat capacity as

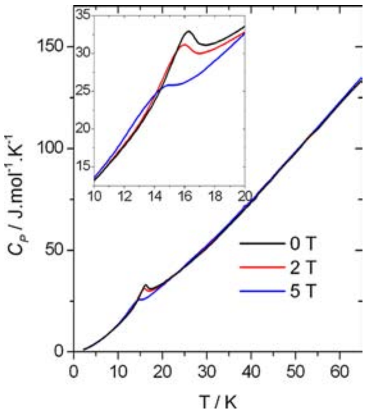

Figure 10. Thermal dependence of the heat capacity (C_P) recorded under various applied dc fields.

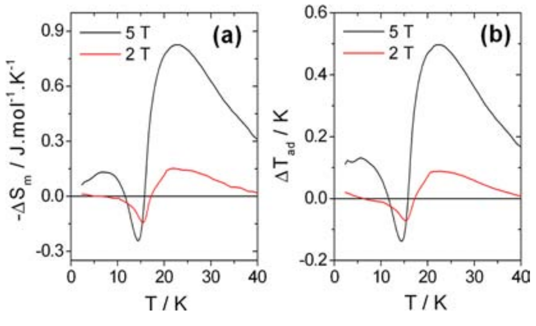

Figure 11. Temperature dependence of the MCE for field variations of 2 and 5 T. (a) Magnetic entropy change. (b) Adiabatic temperature change.

$$S(T) = \int_0^T \frac{C_P(T)}{T} dT + S_0$$

where S_0 is the zero-temperature entropy. When integrating heat capacity data, the missing entropy below 2.3 K (the lowest temperature of the experiment) was taken into account by considering the linear variation of C_P down to 0 K. $\Delta S_M(T)$ is given by the isothermal difference (for a field variation $\Delta H = H_f - H_i$) between the $S(T)_{Hi}$ and $S(T)_{Hf}$ functions:

$$\Delta S_M(T)_{\Delta H} = [S(T)_{H_f} - S(T)_{H_i}]_T$$

while $\Delta T_{ad}(T)$ is calculated as their isentropic difference:

$$\Delta T_{ad}(T)_{\Delta H} = [T(S)_{H_f} - T(S)_{H_i}]_S$$

Because of the onset on the antiferromagnetic ordering, the magnitude of the MCE is quite weak in $Mn_3(OH)_2(C_6H_2O_4S)_2$. The magnetocaloric response is typical of that of an antiferromagnet.[48,51] In the paramagnetic state, the MCE has a positive sign (normal MCE) and increases upon cooling. It abruptly decreases at the antiferromagnetic ordering to reach negative values (inverse MCE) in a certain temperature interval, as often observed in antiferromagnetic materials.

Comparison with the Structures and Magnetic Properties of Other Mn(II) Layered Hybrid Compounds. The set of values so far deduced from the magnetic measurements of $Mn_3(OH)_2(C_6H_2O_4S)_2$ can be compared with those of two compounds for which the magnetism has recently been studied.[52] The two hybrid materials $Mn_2(OH)_2(C_8H_4O_4)$[29] and $Mn(H_2O)_2(C_8H_4O_4)$,[53] have both a layered structure pillared by the bdc linker ($C_8H_4O_4$). This dicarboxylate linker has very common features with the tdc one: except its "linear-shaped" configuration vs the "V-shaped" one of tdc, both ligands have almost the same length and are made of a single aromatic ring bearing two carboxylate functions. This latter similarity manifests through the close interlayer distances of 9.56, 9.93, and 9.32 Å found for the tdc-based hydroxide compound, bdc-based hydroxide compound and bdc-based hydrated compound, respectively. It is of interest to recall the main structural characteristics of the "magnetic layers" found in the two bdc compounds to compare with $Mn_3(OH)_2(C_6H_2O_4S)_2$ (Figure 12). Indeed, the 2D inorganic subnetwork of $Mn_2(OH)_2(C_8H_4O_4)$ presents striking similarities with the one of the presently studied compound. It is also based on two independent metallic sites and consists of an infinite 2D array of vertex-sharing chains of edge-sharing MnO_6 octahedrons. The magnetic structure has revealed that these chains of MnO_6 octahedrons promote ferromagnetic couplings and that they are antiferromagnetically coupled between each other.[52] Thus, we expect that, compared to the bdc-based hydroxide compound, quite similar interactions may develop within the triple-chain ribbon of our new compound. In turn, the "magnetic layers" of $Mn(H_2O)_2(C_8H_4O_4)$ are made of isolated MnO_6 octahedrons connected by the carboxylate function of the interlayer bdc linker,[53] and the neutron diffraction study has shown that the carboxylato-bridges carry antiferromagnetic coupling.[52] We can point out that a compound of similar formula with *p*-phenylenediacrylate in place of bdc has recently been studied.[54]

Therefore, comparing the magnetic properties of these three compounds is of prominent interest. This is done in Table 3 which summarizes their main characteristics. All the values

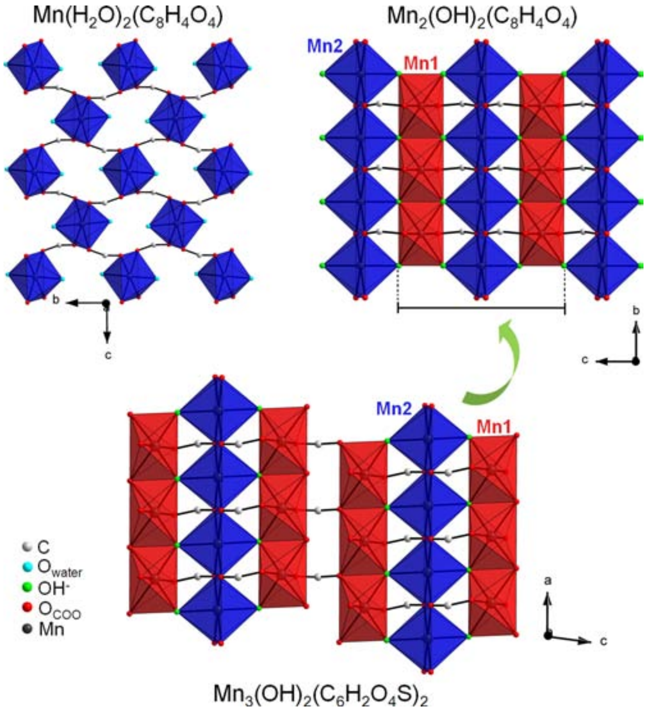

Figure 12. View from the top of the inorganic subnetworks of the layered hybrid compounds $Mn_3(OH)_2(C_6H_2O_4S)_2$, $Mn_2(OH)_2(C_8H_4O_4)$, and $Mn(H_2O)_2(C_8H_4O_4)$. (Mn1 = red and Mn2 = blue, for the two hydroxide compounds).

Table 3. Néel Temperatures, Intralayer Overall Exchange Coupling Constants from the 2D Heisenberg Model Fit, Paramagnetic Temperature from the Curie-Weiss Fit, And Observed Threshold Fields at Low-Temperature for the tdc-Based Compound Studied Here and for the Two bdc-Based Mn(II) Hybrid Magnets

	$Mn(H_2O)_2(bdc)^a$	$Mn_3(OH)_2(tdc)_2$	$Mn_2(OH)_2(bdc)^a$
T_N	6.5 K	17.7 K	38.5 K
J_{intra}	−7.4 K	−44.7 K	−61.5 K
θ_p	−5.2 K	−68.2 K	−99.5
μ_0H_c	1.2 T (at 2 K)	2.9 T (at 5 K)	5.7 T (at 2 K)

[a] Data from ref 52.

deduced from the magnetic measurements presented here for $Mn_3(OH)_2(C_6H_2O_4S)_2$ fall in the interval between those previously found for the two bdc compounds.[52] Drillon and Panissod have demonstrated that, in such kind of layered magnetic systems, the ordering temperature depends only weakly upon the interlayer spacing but is close to the temperature at which the intralayer correlation length diverges.[55] On the basis of this model and the fact that the divergence of the intralayer correlation length mainly depends on the strength of the intralayer interactions, the intermediate Néel temperature found in $Mn_3(OH)_2(C_6H_2O_4S)_2$ can be interpreted as a consequence of the intermediate values evaluated for the two parameters characterizing the intralayer interactions, namely, J_{intra} and θ_p. In a similar way, we note that the threshold field for which a metamagnetic-like behavior is observed is also found to be intermediate between those of the two bdc compounds.

■ CONCLUSIONS

In conclusion, our investigations into the chemistry of MOFs involving dicarboxylate linkers and transition metal elements in basic media have afforded a new compound based on Mn(II) ions and thiophene-2,5-dicarboxylate (tdc). $Mn_3(OH)_2(C_6H_2O_4S)_2$ has a layered structure made of a pseudo-2D inorganic subnetwork of carboxylato-bridged triple chain ribbons which are pillared in the third dimension by the tdc molecules. The tdc ligand exhibits an unprecedented symmetric hexadentate bridging motif, and the 1D inorganic ribbons have striking similarities with the 2D inorganic subnetwork of the parent compound $Mn_2(OH)_2(C_8H_4O_4)$. The differences found between the inorganic subnetwork of $Mn_3(OH)_2(C_6H_2O_4S)_2$ and those of the $M_2(OH)_2(C_8H_4O_4)$ compounds may be considered as being a consequence of the "V-shaped" configuration of tdc, compared with the linear one of bdc. The magnetic properties have been investigated and compared with those of the $Mn_2(OH)_2(C_8H_4O_4)$ and $Mn(H_2O)_2(C_8H_4O_4)$ layered hybrid magnets because the "magnetic layers" of the new $Mn_3(OH)_2(C_6H_2O_4S)_2$ MOF can be considered as intermediate between those of these two compounds. We found that, when compared to the magnetic properties of the two other compounds, those of the new MOF reflect the intermediate topology of its magnetic layers.

We are currently working on the determination of the magnetic structure of $Mn_3(OH)_2(C_6H_2O_4S)_2$ by means of neutron diffraction experiments. A preliminary experiment suggests that the magnetic structure is incommensurate, but other measurements are needed to solve the magnetic structure. In comparison with the commensurate magnetic structures of $Mn_2(OH)_2(C_8H_4O_4)$ and $Mn(H_2O)_2(C_8H_4O_4)$, this particularity may result from the arrangement of the $S = 5/2$ spins within the pseudo-2D inorganic subnetwork of the present compound.

■ ASSOCIATED CONTENT

Ⓢ Supporting Information

A photograph of the compound, the TGA trace, the final geometry of the tdc molecule resulting from the XRPD data refinement, additional structure drawings, a table gathering all the coordination modes of the ligand, and the atomic coordinates. This material is available free of charge via the Internet at http://pubs.acs.org.

■ AUTHOR INFORMATION

Corresponding Author

*E-mail: rom.sibille@gmail.com.

Notes

The authors declare no competing financial interest.

■ ACKNOWLEDGMENTS

The SOLEIL synchrotron (Saint Aubin, France) is warmly acknowledged for the allocated beam time. We thank Lionel Aranda (Institut Jean Lamour, Nancy) for TG measurements. We are very grateful to Bernard Monod (LEMTA, Nancy) for his help with FTIR measurements.

■ REFERENCES

(1) (a) Tranchemontagne, D. J.; Mendoz-Cortes, J. L.; O'Keeffe, M.; Yaghi, O. M. *Chem. Soc. Rev.* **2009**, *38*, 1257−1283. (b) Horike, S.; Shimomura, S.; Kitagawa, S. *Nat. Chem.* **2009**, *1*, 695−704. (c) Ferey, G. *Chem. Soc. Rev.* **2008**, *37*, 191−214.

(2) (a) Rosi, N. L.; Kim, J.; Eddaoudi, M.; Chen, B.; O'Keeffe, M.; Yaghi, O. M. *J. Am. Chem. Soc.* **2005**, *127*, 1504−1518. (b) Eddaoudi, M.; Kim, J.; Rosi, N. L.; Vodak, D.; Wachter, J.; O'Keeffe, M.; Yaghi, O. M. *Science* **2002**, *295*, 469−475. (c) Eddaoudi, M.; Kim, J.; Rosi, N. L.; Vodak, D.; Sudik, J.; Wachter, J.; O'Keeffe, M.; Yaghi, O. M. *Proc. Natl. Acad. Sci. U.S.A.* **2002**, *99*, 4900−4904. (d) Eddaoudi, M.; Moler, D. B.; Li, H.; Chen, B.; Reineke, T. M.; O'Keeffe, M.; Yaghi, O. M. *Acc. Chem. Res.* **2001**, *34*, 319−330. (e) Rowsell, J. L. C.; Yaghi, O. M. *Angew. Chem., Int. Ed.* **2005**, *44*, 4670−4679. (f) Férey, G.; Mellot-Draznieks, C.; Serre, C.; Millange, F.; Dutour, J.; Surblé, S.; Margiolaki, I. *Science* **2005**, *309*, 2040−2042. (g) Férey, G.; Mellot-Draznieks, C.; Serre, C.; Millange, F.; Dutour, J.; Surblé, S.; Margiolaki, I. *Science* **2005**, *309*, 2040−2042.

(3) Pan, L.; Liu, H.; Lei, X.; Huang, X.; Olson, D. H.; Turro, N. J.; Li, J. *Angew. Chem., Int. Ed.* **2003**, *42*, 542−546.

(4) Chen, B.; wang, L.; Zapata, F.; Qian, G.; Lobkovsky, E. B. *J. Am. Chem. Soc.* **2008**, *8*, 6718−6719.

(5) (a) Xue, M.; Zhu, G.; Li, Y.; Zhao, X.; Jin, Z.; Kang, E.; Qiu, S. *Cryst. Growth. Des.* **2008**, *8*, 2478−2483. (b) Zhang, L.; Qin, Y. Y.; Li, Z. J.; Lin, Q. P.; Cheng, J. K.; Zhang, J.; Yao, Y. G. *Inorg. Chem.* **2008**, *47*, 8286−8293.

(6) (a) Weng, D. F.; Wang, Z. M.; Gao, S. *Chem. Soc. Rev.* **2011**, *40*, 3157−3181. (b) Dechambenoit, P.; Long, J. R. *Chem. Soc. Rev.* **2011**, *40*, 3249−3265. (c) Miller, J. S. *Chem. Soc. Rev.* **2011**, *40*, 3266−3296. (d) Kurmoo, M. *Chem. Soc. Rev.* **2009**, *38*, 1353−1379. (e) Huang, Z. L.; Drillon, M.; Masciocchi, N.; Sironi, A.; Zhao, J. T.; Rabu, P.; Panissod, P. *Chem. Mater.* **2000**, *12*, 2805−2812.

(7) (a) Rueff, J. M.; Masciocchi, N.; Rabu, P.; Sironi, A.; Skoulios, A. *Chem.—Eur. J.* **2002**, *8*, 1813−1820. (b) Guillou, N.; Livage, C.; Férey, G. *Eur. J. Inorg. Chem.* **2006**, *24*, 4963−4978. (c) Mesbah, A.; Carton, A.; Aranda, L.; Mazet, T.; Porcher, F.; François, M. *J. Solid. State Chem.* **2008**, *181*, 3229−3235.

(8) Sibille, R.; Mazet, T.; Malaman, B.; Gaudisson, T.; François, M. *Inorg. Chem.* **2012**, *51*, 2885−2892.

(9) (a) Kitagawa, S.; Kitaura, R.; Noro, S. I. *Angew. Chem., Int. Ed.* **2004**, *43*, 2334−2375. (b) Maspoch, D.; Ruiz-Molina, D.; Veciana, J. *Chem. Soc. Rev.* **2007**, *36*, 770−818. (c) Férey, G.; Mellot-Draznieks, C.; Serre, C.; Millange, F. *Acc. Chem. Res.* **2005**, *38*, 217−225. (d) Bradshaw, D.; Claridge, J. B.; Cussen, E. J.; Prior, T. J.; Rosseinsky, M. J. *Acc. Chem. Res.* **2005**, *38*, 273−282. (e) Janiak, C. *Dalton. Trans.* **2003**, *38*, 2781−2804.

(10) Yuan, L.; Li, Z.; Sun, J.; Zhang, K. *Spectrochim. Acta, Part A* **2003**, *59*, 2949−2953.

(11) (a) Cai, L. Z.; Chen, W. T.; Wang, M. S.; Guo, G. C.; Huang, J. S. *Inorg. Chem. Commun.* **2004**, *7*, 611−613. (b) Yin, M. C.; Yuan, L. J.; Ai, C. C.; Wang, C. W.; Yuan, E. T.; Sun, J. T. *Polyhedron* **2004**, *23*, 529−536. (c) Teotonio, E. E. S.; Felinto, M. C. F. C.; Brito, H. F.; Malta, O. L.; Trindade, A. C.; Najjar, R.; Strek, W. *Inorg. Chim. Acta* **2004**, *357*, 451−460.

(12) Yuan, L.; Yin, M.; Yuan, E.; Sun, J. *Inorg. Chim. Acta* **2004**, *357*, 89−94.

(13) Huang, W.; Wu, D.; Zhou, P.; Yan, W.; Guo, D.; Duan, C.; Meng, Q. *Cryst. Growth. Des.* **2009**, *9*, 1361−1369.

(14) Wang, J. G.; Huang, C. C.; Huang, X. H.; Liu, D. S. *Cryst. Growth. Des.* **2008**, *8*, 795−798 3.

(15) Xu, J.; Cheng, J.; Su, W.; Hong, M. *Cryst. Growth. Des.* **2011**, *11*, 2294−2301.

(16) Wang, M. X.; Long, L. S.; Huang, R. B.; Zheng, L. S. *Chem. Commun.* **2011**, *47*, 9834−9836.

(17) Demessence, A.; Rogez, G.; Rabu, P. *Chem. Mater.* **2006**, *18*, 3005−3015.

(18) (a) Demessence, A.; Yassar, A.; Rogez, G.; Miozzo, L.; De Brion, S.; Rabu, P. *J. Mater. Chem.* **2010**, *20*, 9401−9414. (b) Rogez, G.; Massobrio, C.; Rabu, P.; Drillon, M. *Chem. Soc. Rev.* **2011**, *40*, 1031−1058.

(19) Demessence, A.; Mesbah, A.; François, M.; Rogez, G.; Rabu, P. *Eur. J. Inorg. Chem.* **2009**, *25*, 3713−3720.

(20) Demessence, A.; Rogez, G.; Welter, R.; Rabu, P. *Inorg. Chem.* **2007**, *46*, 3423−3425.

(21) Haryono, M.; Kalisz, M.; Sibille, R.; Lescouëzec, R.; Fave, C.; Trippe-Allard, G.; Li, Y.; Seuleiman, M.; Rousselière, H.; Balkhy, A. M.; Lacroix, J. C.; Journaux, Y. *Dalton Trans.* **2010**, *46*, 3423−3425.

(22) Yuan, H. B.; Yang, S. Y.; Xie, Z. X.; Huang, R. B.; Batten, S. R. *Inorg. Chem. Commun.* **2009**, *39*, 4751−4756.

(23) Chen, B. L.; Mok, K. F.; Ng, S. C.; Drew, G. B. *New J. Chem.* **1999**, *23*, 877−883.

(24) Zou, H. H.; He, Y. P.; Gui, L. C.; Liang, F. P. *CrystEngComm.* **2011**, *13*, 3325−3329.

(25) Jia, H. P.; Li, W.; Ju, Z. F.; Zhang, J. *Eur. J. Inorg. Chem.* **2006**, 4264−4270.

(26) Sun, X. Z.; Sun, Y. F.; Ye, B. H.; Chen, X. M. *Inorg. Chem. Commun.* **2003**, *6*, 1412−1414.

(27) Han, K. F.; Wang, D.; Wang, Z. M. *Acta Crystallogr.* **2007**, *E63*, m1333−m1334.

(28) Yesilel, O. Z.; Ilker, I.; Sahin, E. *J. Inorg. Organomet. Polym.* **2011**, *21*, 103−109.

(29) (a) Huang, Z. L.; Drillon, M.; Masciocchi, N.; Sironi, A.; Zhao, J. T.; Rabu, P.; Panissod, P. *Chem. Mater.* **2000**, *12*, 2805−2812. (b) Abdelouhab, S.; François, M.; Elkaïm, E.; Rabu, P. *Sol. State Sci.* **2005**, *7*, 227−232. (c) Carton, A.; Abdelouhab, S.; Renaudin, G.; Rabu, P.; François, M. *Sol. State Sci.* **2006**, *8*, 958−963. (d) Carton, A.; Mesbah, A.; François, M.; Rabu, P. *Z. Kristallogr. Suppl.* **2007**, *26*, 581−586.

(30) Rodriguez-Carvajal, J. *Phys. B.* **1993**, *55*, 192.

(31) Werner, P. E.; Eriksson, L.; Westdhal, M. *J. Appl. Crystallogr.* **1975**, *8*, 372−374.

(32) Boultif, A.; Louer, D. *J. Appl. Crystallogr.* **2004**, *37*, 724−731.

(33) Le Bail, A.; Duroy, H.; Fourquet, J. L. *Mater. Res. Bull.* **1988**, *23*, 447−452.

(34) Favre-Nicolin, V.; Cerny. *J. Appl. Crystallogr.* **2002**, *35*, 734−743.

(35) *Fox, Free Objects for Crystallography*; http://objcryst.sourceforge.net

(36) (a) Cheetham, A. K.; Rao, C. N. R.; Feller, R. K. *Chem. Commun.* **2006**, 4780−4795. (b) Rao, C. N. R.; Cheetham, A. K.; Thirumurugan, A. *J. Phys.: Condens. Matter.* **2008**, *20*, 083202.

(37) Chen, B. L.; Mok, K. F.; Ng, S. C.; Feng, Y. L.; Liu, S. X. *Polyhedron* **1998**, *17*, 4237−4247.

(38) Chen, B. L.; Mok, K. F.; Ng, S. C.; Drew, M. G. B. *Polyhedron* **1999**, *18*, 1211−1220.

(39) Byrnes, M. J.; Chisholm, M. H. *Chem. Commun.* **2002**, 2040−2041.

(40) Byrnes, M. J.; Chisholm, M. H.; Clark, R. J. H.; Gallucci, J. C.; Hadad, C. M.; Patmore, N. J. *Inorg. Chem.* **2004**, *43*, 6334−6344.

(41) Zhao, L.; Liang, J.; Yue, G.; Deng, X.; He, Y. *Acta Crystallogr.* **2009**, *E65*, m722.

(42) Yesilel, O. Z.; Ilker, I.; Büyükgüngor, O. *Polyhedron* **2009**, *28*, 3010−3016.

(43) Sun, X. Z.; Huag, Z. L.; Wang, H. Z.; Ye, B. H.; Chen, X. M. *Z. Anorg. Allg. Chem.* **2006**, *631*, 919−923.

(44) The topological analysis has been done by using the TOPOS 4.0 program: Blatov, V. A. *IUCr CompComm. Newsletter* **2006**, *7*, 4−38.

(45) (a) Suzuki, F.; Shibata, N.; Ishii, C. *J. Phys. Soc. Jpn.* **1994**, *63*, 1539. (b) Souletie, J.; Rabu, P.; Drillon, M. In *Magnetism: Molecules to Materials, V*; Miller, J. S., Drillon, M., Eds.; Wiley-VCH: Weinheim, Germany, 2005; pp 347−377. (c) Bauer, E. M.; Bellitto, C.; Righini, G.; Colapietro, M.; Portalone, G.; Drillon, M.; Rabu, P. *Inorg. Chem.* **2008**, *47*, 10945−10952.

(46) Sengupta, P.; Sandvik, A. W.; Singh, R. R. P. *Phys. Rev. B* **2003**, *68*, 094423.

(47) (a) Blanco, J. A.; Gignoux, D.; Schmitt, D. *Phys. Rev. B* **1991**, *43*, 13145. (b) Bouvier, M.; Lethillier, P.; Schmitt, D. *Phys. Rev. B* **1991**, *43*, 13137.

(48) Tishin, A. M.; Spichkin, Y. I. *The Magnetocaloric Effect and its Applications*; IOP Publishing: Bristol, U.K., 2003.

(49) (a) Shiron, P. J. *J. Low Temp. Phys.* **2007**, *148*, 915. (b) Sibille, R.; Mazet, T.; Malaman, B.; Francois, M. *Chem. Eur. J.* **2012**, *18*, 12970−12973.

(50) Pecharsky, V. K.; Gschneidner, K. A., Jr. *J. Appl. Phys.* **1999**, *86*, 565−575.

(51) von Ranke, P. J.; de Oliveira, N. A.; Alho, B. P.; Plaza, E. J. R.; de Sousa, V. S. R.; Caron, L.; Reis, M. S. *J. Phys. Condens. Matter* **2009**, *21*, 056004.

(52) Sibille, R.; Mesbah, A.; Mazet, T.; Malaman, B.; Capelli, S.; François, M. *J. Solid State. Chem.* **2012**, *186*, 134−141.

(53) Kaduk, J. A. *Acta Crystallogr.* **2002**, *B58*, 815.

(54) Sun, Q.; Cheng, A. L.; Wang, Y. Q.; Ma, Y.; Gao, E. Q. *Inorg. Chem.* **2011**, *50*, 8144−8152.

(55) (a) Drillon, M.; Panissod, P. *J. Magn. Magn. Mater.* **1998**, *188*, 93−99. (b) Panissod, P.; Drillon, M. In *Magnetism: Molecules to Materials, IV*; Miller, J. S., Drillon, M., Eds.; Wiley-VCH: Weinheim, Germany, 2002; pp 233−269.